Precision Engineering 53 (2018) 79–95

Contents lists available at ScienceDirect

Precision Engineering

journal homepage: www.elsevier.com/locate/precision

Detection and monitoring of defects on three-dimensional curved surfaces based on high-density point cloud data

Delin Huang[a,b], Shichang Du[a,b,*], Guilong Li[a,b], Chen Zhao[a,b], Yafei Deng[a,b]

[a] State Key Lab of Mechanical System and Vibration, Shanghai Jiao Tong University, Shanghai, 200240, China
[b] School of Mechanical Engineering, Shanghai Jiao Tong University, Shanghai, 200240, China

ARTICLE INFO

Keywords:
Defect detection and monitoring
High-density point cloud data
Three-dimensional curved surface

ABSTRACT

The surface quality of three-dimensional (3-D) curved surfaces is one of the most important factors that can directly influence the performance of the final product. This paper presents a systematic approach for detection and monitoring of defects on 3-D curved surfaces based on high-density point cloud data. Firstly, an algorithm to remove outliers and a boundary recognition algorithm are proposed to divide the entire 3-D curved surface including millions of measured points into multiple sub-regions. Secondly, two new evaluation indexes based on wavelet packet entropy and normal vector are explored to represent the features of the multiple sub-regions to determine whether the sub-regions are out-of-limit (OOL) of specifications. Thirdly, three quality parameters representing quality characteristics of a curved surface are presented and their values are calculated based on the clusters of OOL sub-regions. Finally, three individual control charts are presented to monitor the three quality parameters. As long as any quality parameter is out of the control range, the manufacturing process of the curved surface is determined to be out-of-control (OOC). The results of a case study show that the proposed approach can effectively identify the OOC manufacturing process and detect defects on 3-D curved surfaces.

1. Introduction

The surface quality of three-dimensional (3-D) curved surfaces is very important for product performance. For instance, the inner surface of an engine cylinder head combustion chamber is a 3-D curved surface. If the inner surface is defective, the volume of the combustion chamber will be affected and in turn one of the significant performances of an engine, namely, compression ratio, will be affected greatly. The traditional quality control method of the inner surface is applied based on coordinate measurement machine (CMM). Although CMM is high in accuracy, the number of measured points is small and the entire surface contour cannot be fully reflected. With the development of high definition metrology (HDM) technologies, high-density point cloud data is measured for reflection of the entire curved surface contour (see Fig. 1), which provides great opportunities for quality control of 3-D curved surfaces. About one million measurement points are collected from a cylinder head by HDM system [1].

Many researches have been conducted on detection and monitoring of defects on flat surfaces. Wang et al. [2] employed the fused least absolute shrinkage and selection operator (LASSO) algorithm to identify potentially shifted sites on wafer surfaces and proposed a variable selection-based statistical process control (SPC) method for monitoring two-dimensional (2-D) data maps. He et al. [3] proposed a multivariate generalized likelihood ratio (MGLR) control chart for monitoring and detecting numerous number of fault clusters per image in industrial applications. Sullivan [4] proposed a method based on profile monitoring which is effective in detecting single or multiple shifts and/or outliers and described the algorithm and an effective stopping rule that controlled the false detection rate. Woodall et al. [5] reviewed the monitoring methods of process and product profiles (representation of quality characteristics) in statistical process control and exhibited comparisons of the monitoring methods for linear calibration relationships, change-point methods for simple linear regression profile data, and the use of generalized linear models to represent profiles. However, profile monitoring is based on the assumption that the can be represented by linear, nonlinear or nonparametric model.

With the development of measurement technologies, several researches about controlling flat surface variation based on HDM have also been conducted. Du et al. [6–8] proposed a shearlet-based method and support vector machine-based methods to separate and extract different surface components using HDM. Du et al. [9] presented a co-Kriging method based on multivariate spatial statistics to estimate surface form error. Du et al. [10] also developed a fast and adaptive bi-dimensional empirical mode decomposition (FABEMD) approach for

* Corresponding author at: State Key Lab of Mechanical System and Vibration, Shanghai Jiao Tong University, Shanghai, 200240, China.
E-mail address: lovbin@sjtu.edu.cn (S. Du).

https://doi.org/10.1016/j.precisioneng.2018.03.001
Received 6 June 2017; Received in revised form 27 January 2018; Accepted 1 March 2018
Available online 10 March 2018
0141-6359/

Fig. 1. The high-density point cloud data of a curved surface of an engine cylinder head.

filtering of workpiece surfaces using HDM. Wang et al. [11–13] developed a modified gray level co-occurrence matrix to extract features from the images converted from face-milled surface measured by HDM. Suriano et al. [14] proposed a new methodology for efficiently measuring and monitoring flat surface variations by fusing in-plant multi-resolution measurements and process information. Nguyen et al. [15] presented a method to reduce flat surface variation in face milling processes based on HDM. Wells et al. [16] proposed an adaptive generalized likelihood ratio (AGLR) technique to monitor the planar surface defects by transforming high-density data into a grayscale image.

However, the above researches based on HDM only focus on the flat surface. It is desired to develop a systematic approach for detection and monitoring of defects on 3-D curved surface based on high-density point cloud data. Since the number of the curved surface point cloud data is large, it is unrealistic to directly monitor the entire surface quality by monitoring the condition of each point. Wang et al. [17] used quantile–quantile (Q–Q) plot to characterize a huge sample and transform it to a linear profile, and proposed profile monitoring techniques to improve the performance of a conventional control chart. Wells et al. [18] also used Q–Q plots to transform high-density point cloud data into linear profiles that can be monitored by well-established profile monitoring techniques. But the methods using Q–Q plot cannot identify the locations of defective regions from the curved surface in out-of-control (OOC) condition. Colosimo et al. [19] developed a method consisting of modeling the manufactured surface via Gaussian processes models and monitoring the deviations of the actual surface from the target pattern estimated in Phase I. The proposed method is limited to monitoring surfaces (for example a cylindrical surface) characterized by parametric models.

In this paper, the curved surface is divided into hundreds of small sub-regions, and each small sub-region contains dozens of 3-D points. The defects of the small sub-region are characterized by two explored evaluation indexes: the non-random distribution of abnormal points (NDAP) of a sub-region and the plane direction deviation (PDD) of a sub-region. The NDAP is calculated by the wavelet packet entropy and the PDD is calculated by the normal vector. The wavelet packet coefficients are used to extract the NDAP feature of a sub-region, which are quantified by the information entropy. That is, the wavelet packet entropy is used as the NDAP feature of each sub-region. In order to accurately extract the PDD features of the divided sub-regions, the normal vector of each sub-region is also calculated. Wavelet packet entropies and normal vectors of the modulus curved surface are calculated as the criteria to evaluate whether the sub-regions of the measured curved surface are out-of-limit (OOL). When the OOL sub-regions are identified, three quality parameters that represent quality characteristics of the measured curved surface are calculated based on the clusters of OOL sub-regions. Three individual control charts are made to monitor the three quality parameters.

The remainder of this paper is organized as follows. In Section 2, a systematic approach is proposed to detect and monitor defects on 3-D curved surface based on high-density point cloud data. In Section 3, a case study is presented to validate the proposed approach. The result analysis is implemented to illustrate the performance of the proposed approach for detection and monitoring of defects on 3-D curved surfaces. Finally, conclusions are given in Section 4.

2. The proposed approach

2.1. Framework

This sub-section presents an overview of the proposed approach for monitoring 3-D curved surface quality of a workpiece based on high-density point cloud data. The framework of the proposed approach is shown in Fig. 2. The procedure involves the following steps.

Step 1: Region division of curved surfaces. HDM is employed to collect 3-D coordinates from workpiece surfaces. The curved surface (represented by the measured point cloud data) is divided into multiple sub-regions through remove of outlier, boundary recognition and sub-region division. A sub-region is a small point cloud (usually consisting of dozens or hundreds of 3-D points) that represents a part of the curved surface. In order to evaluate the quality of each divided sub-region, the modulus point cloud data (i.e., product design specification) of the curved surface is processed by boundary recognition and sub-region division.

Step 2: Feature evaluation of each sub-region. Two new evaluation indexes (NDAP and PDD) based on wavelet packet entropies and normal vectors are explored to represent the features of sub-regions of the measured curved surface. Wavelet packet entropies and normal vectors of sub-regions of the modulus curved surface also need to be calculated as the criteria.

Step 3: Quality parameters calculation of the curved surface. When the OOL sub-regions of the measured curved surface are recognized, three quality parameters that represent quality characteristics of the measured curved surface are calculated by clusters of the OOL sub-regions.

Step 4: Monitoring the three quality parameters. Each quality parameter is monitored by an individual control chart. If any quality parameter of a curved surface is out of the control range, the manufacturing process is OOC and the correction should be conducted.

2.2. Region division of curved surfaces

2.2.1. Algorithm to remove outliers

Due to the interference of the measurement environment and the surface reflection of the measured workpiece, etc., there are mainly outliers in the measured point cloud data (the measured curved surface). There are three types of outliers: the outliers generated by ambient light interference, the outliers caused by the reflective properties of the curved surface of a workpiece, and the outliers that are not obvious. An algorithm including three steps is proposed to remove the corresponding type of outliers.

Step 1: Remove the outliers generated by ambient light interference. Since the maximum distance from the surface to the bottom of a workpiece is known, the maximum distance is set as the distance threshold to determine whether a point is an outlier. If the Z coordinate value of a point is greater than the distance threshold, the point is

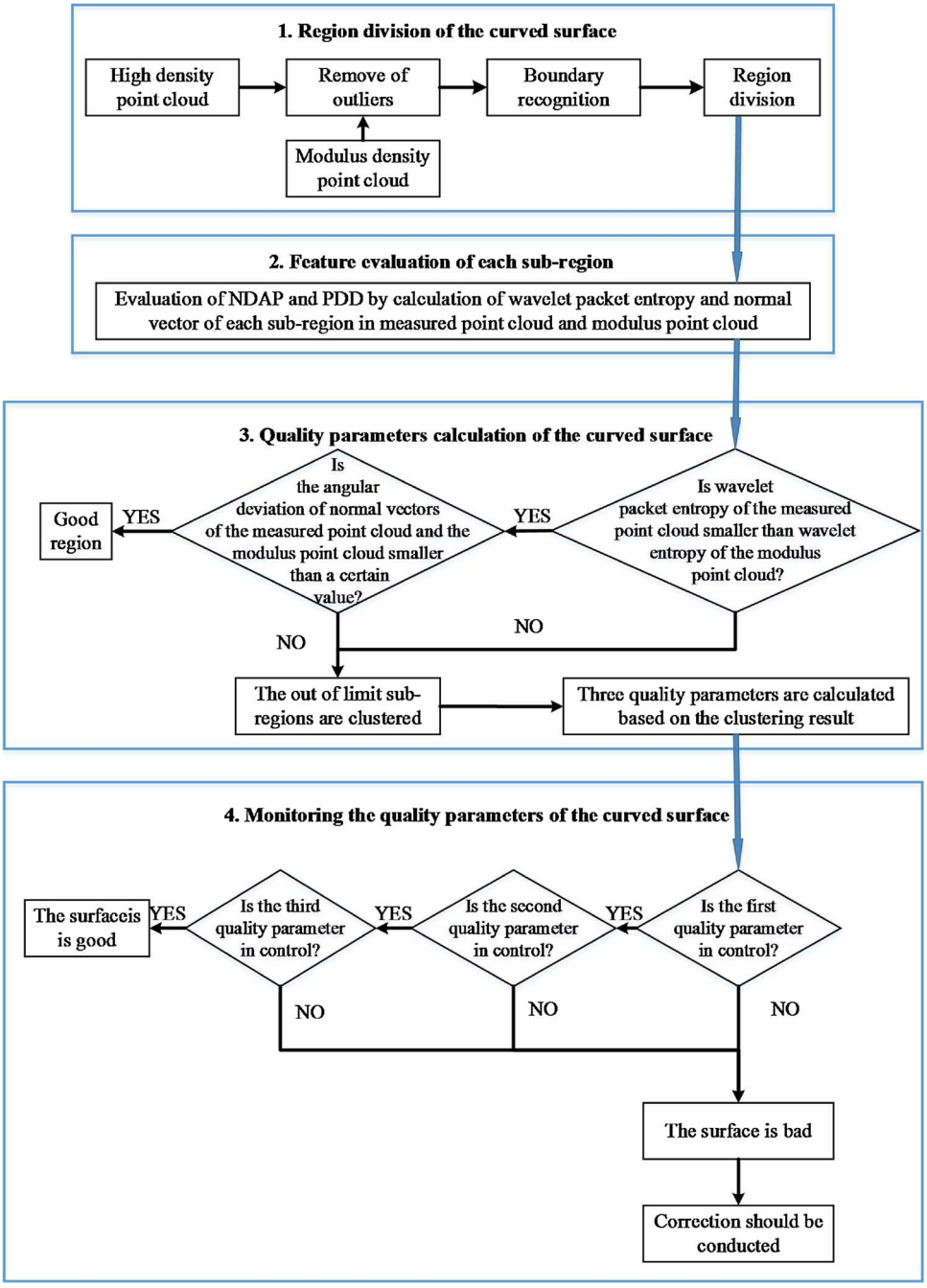

Fig. 2. Framework of the proposed approach.

regarded as an outlier. In order to keep the ordered structure of the measured point cloud data, the recognized outliers are replaced by coordinates of [*x*; *y*; *na*]. Here, *x* and *y* are the corresponding coordinate values of the recognized outliers, while *na* means the Z coordinate value is removed.

Step 2: Remove the outliers caused by the reflective properties of the surface of the workpiece. This type of outliers indicates features of small number and isolation. Mark the missing points of the point cloud data (shown in Fig. 3) and outliers recognized in Step 1 as null values, and count the number of non-null points between adjacent points marked as null values. If the number is smaller than a set threshold, the non-null points are regarded as outliers and should be removed. In addition, the points marked as null and points to be removed should be replaced by coordinates of [*x*; *y*; *na*].

Step 3: Further remove the unobvious outliers using *K*-nearest

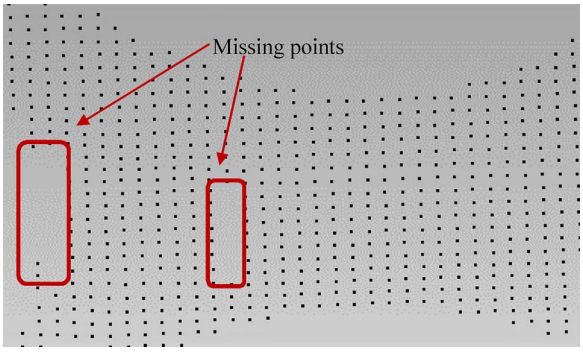

Fig. 3. Missing points in the measured point cloud data.

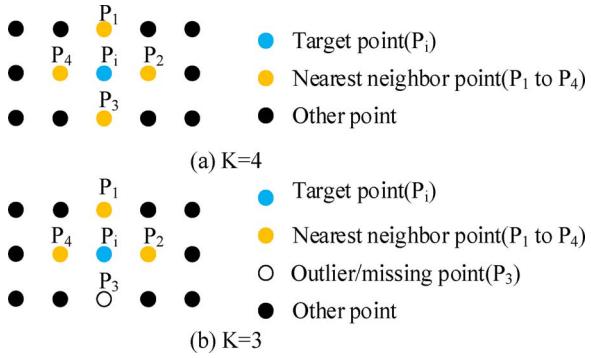

Fig. 4. The *K*-nearest neighbor points of a target point.

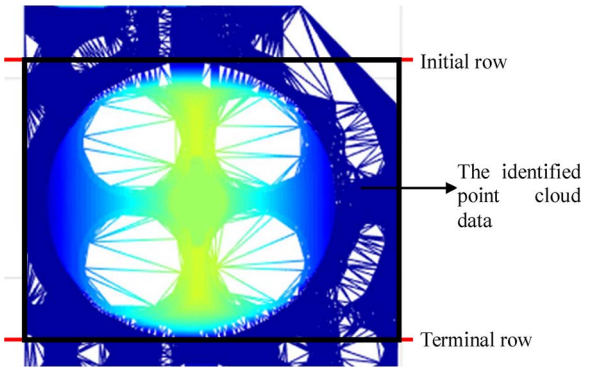

Fig. 6. Determination of initial/terminal row of the curved surface point cloud data.

neighbor algorithm based on statistics. For a point (P_i) of the point cloud, count the nearest K points (P_{i1}, P_{i2} …, P_{iK}) of point P_i and calculate the distance (d_{i1}, d_{i2}…, d_{iK}) between point P_i and its K-nearest neighbor points. The average distance of the K-nearest neighbor points of the point P_i is calculated as$dMean_i = \sum_{j=1}^{K} d_{ij}/K$. Since the structure of the measured point cloud data is ordered, the nearest neighbor points of point P_i are P_1, P_2, P_3, and P_4 (shown in Fig. 4), and K is determined as 4. Considering the fact that the nearest neighbor points may contain outliers or missing points (shown in Fig. 4 (b)), the value of K is usually determined as $K \leq 4$. The average distance of the point cloud is calculated as$dist = \sum_{i=1}^{Num} dMean_i/Num$, and the mean square error is calculated as$\sigma = \sqrt{\frac{1}{Num}\sum_{i=1}^{Num}(dist - dMean_i)^2}$. Here, *Num* is the number of all points of the curved surface point cloud data. Since the average distance (*dMean*) of each point of the curved surface point cloud data is in accordance with the 3σ law of the Gaussian distribution, the outliers do not satisfy the 3σ law of the Gaussian distribution. Set [dist−3σ, dist + 3σ] as the standard interval and remove the points with $dMean_i$ that does not conform to the standard interval. Coordinate of [*x*; *y*; *na*] is also used to replace the removed points to keep the ordered structure of the measured point cloud data.

2.2.2. Boundary recognition algorithm

The measured point cloud data of a workpiece contains usually plane point cloud data and curved surface point cloud data. A curved surface has boundary, which needs to be recognized from the measured point cloud. According to the fact that Z coordinate values of the points in the plane and the curved surface are quite different, the initial/terminal row and initial/terminal column of the curved surface point cloud data is obtained. The boundary recognition algorithm of identifying the curved surface point cloud data from the measured point cloud data is described as follows.

Step 1: Since the structure of the measured point cloud data is ordered, the rows and columns of the measured point cloud data are marked (shown in Fig. 5).

Step 2: Calculate the mean of the Z-coordinate values of each row, determine the serial numbers of the initial and terminal rows according to the change of average Z-coordinate value, and store all the points from the initial row to the terminal row. The stored points are regarded as the selected point cloud data (shown in Fig. 6).

Step 3: Calculate the mean of Z-coordinate values of each column of the selected point cloud data, and determine the serial numbers of the initial and terminal columns according to the change of average Z coordinate values. The location of curved surface point cloud data is shown in Fig. 7.

Step 4: Identify the curved surface point cloud data. Although the location of the curved surface point cloud data has been identified, the identified point cloud data in rectangular region (shown in Fig. 7) also contains the plane point cloud data. According to the difference of Z coordinate values of the points in the plane and the curved surface, the points in the plane that are within the initial/terminal row and initial/terminal column are selected. In order to ensure that each row/column contains the same number of points, these selected points should be replaced by coordinates of [*x*; *y*; 0] instead of being deleted.

2.2.3. Sub-region division

The identified point cloud data in sub-section 2.2.2 is regarded as the curved surface point cloud data since the coordinates of the plane points included in the identified point cloud data are marked as [000]. In order to monitor the curved surface quality of a workpiece, the curved surface is divided into $M \times N$ (M and N should be integers) sub-regions. Each sub-region contains a small number of points (dozens of points). Assume that the serial number of the initial and terminal rows are m_1 and m_2, and the serial number of the initial and terminal columns are n_1 and n_2. Then the curved surface point cloud data contains (m_2-m_1+1) rows and (n_2-n_1+1) columns.

Step 1: Divide the curved surface into M sub-regions according to the row. Assume that INT[(m_2-m_1+1)/M] = m_3, and m_4 = (m_2-m_1+1)-$M \times m_3$ (the reminder of (m_2-m_1+1) divided by M). Each of the former m_4 sub-regions contains (m_3+1) rows, and the each of the latter (M-m_4)

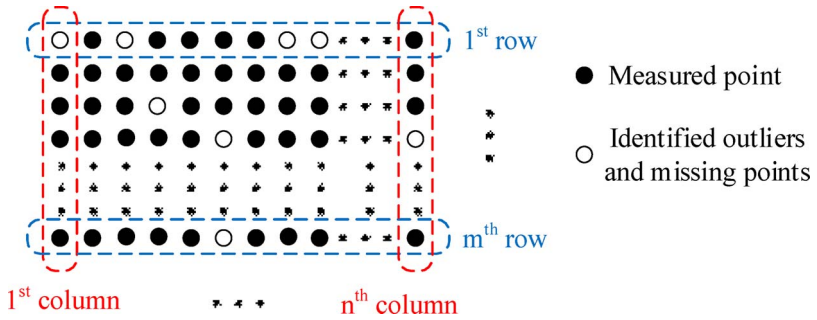

Fig. 5. The structure of the measured point cloud.

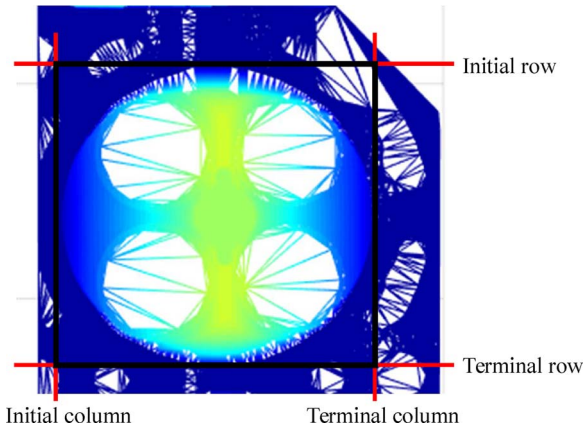

Fig. 7. Location of the curved surface point cloud data.

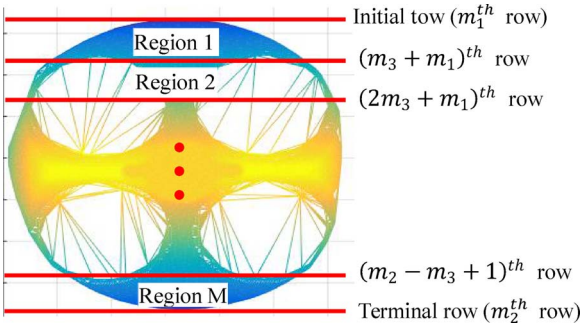

Fig. 8. *M* divided sub-regions of the curved surface point cloud data.

sub-regions contains m_3 rows. An example is shown in Fig. 8.

Step 2: Divide each of the *M* sub-regions into *N* sub-regions according to the column. The process of the division is the same as the previous process shown in Step 1 of Sub-section 2.2.3. The division of the curved surface is shown in Fig. 9.

2.3. Feature evaluation of each sub-region

The defects of the divided sub-regions are identified by two new evaluation indexes of NDAP and PDD based on wavelet packet entropy and normal vector. The NDAP is used to evaluate the random distribution of abnormal points in the sub-region. If the distribution of abnormal points in the sub-region is not random, the NDAP of the sub-region is relatively large and thus the sub-region is considered to be bad. Although the sub-region is good based on the evaluation of the NDAP, the spatial location of the sub-region may not be qualified, which is evaluated by PDD. When both features of the sub-region are qualified, the sub-region is good. The calculation of NDAP and PDD is shown in Fig. 10. The NDAP feature is represented by wavelet packet entropy and the PDD feature is represented by normal vector.

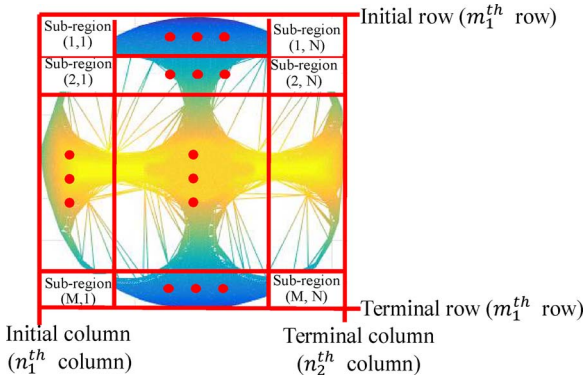

Fig. 9. The sub-region division of the curved surface.

2.3.1. Wavelet packet entropy

Wavelet transform reflects the energy distribution of the data in the time-frequency domain [20,21]. But wavelet transform only decomposes the low frequency components of the data (shown in Fig. 11(a)), which ignores the information of high frequency components. The wavelet packet transform decomposes not only the low frequency components of the signal but also the high frequency components (shown in Fig. 11(b)), which is better applied for feature extraction [22].

Entropy is used to describe and measure the uncertainty of the random variable, and can accurately characterize information. Therefore, the combination of wavelet packet and entropy (wavelet packet entropy) is considered to make full use of their advantages in feature evaluation.

For a regular set of data (e.g. a set of single-frequency data), its relative wavelet packet energy is very small since all the energy is only concentrated on a band. The energy of a very complex data (e.g. a random data) will be distributed in each band, and the relative wavelet packet energy will be relatively similar, which makes wavelet packet entropy maximum. Similarly, wavelet packet entropy is used as the measurement of information of the surface morphology, and it represents the randomness and complexity of the surface morphology. If the quality of workpiece surface is good, the height distribution of each point is regular and non-random, the energy distributions in the time-frequency domain are relatively concentrated in the low frequency band (e.g. AAA_3 in Fig. 11(b)), and the entropy is small. If the points are completely equal, the entropy is zero. On the contrary, if the quality of the surface is bad, the surface heights (Z coordinate values of all points of the surface) distribute randomly and wavelet packet is used for multi-scale analysis of the surface, amplitude and energy of the decomposed components on other scales will increase and the entropy will be relatively large.

The calculation of wavelet packet entropy is conducted based on wavelet packet transform of the surface. The coefficient matrix of the wavelet pocket transform is processed into a probability distribution sequence, and the entropy calculated from it reflects the randomness and complexity of the surface morphology. The procedure of calculating wavelet entropy of each divided sub-region is described as follows.

Step 1: Datum transformation of sub-regions and interpolation. The sub-regions are inclined planes, but current wavelet packet decompositions (1-D and 2-D wavelet packet transforms) cannot be directly used for feature extraction of the inclined planes. Therefore, the datums of the inclined sub-regions need to be transformed into the flat planes. The transformation is shown in Fig. 12 and the specific details can refer to [1]. Since there are sub-regions that only contain few points and the spatial distribution of these points is not a rectangle, rectangular regions should be re-selected from these sub-regions and several points are deleted, which would result in information loss of the re-selected sub-regions. In order to reduce the information loss, interpolation is applied to add the number of points to be decomposed. The interpolation is triangle-based cubic interpolation and the details can refer to [23].

Step 2: Select input data for wavelet packet decomposition. The distribution of points of each divided sub-region is usually not a regular rectangle, which cannot be directly decomposed by wavelet packet.

The regional point cloud data before and after interpolation is the same in distribution (both are not regular rectangles), so it is necessary to select the rectangular data from the regional point cloud data after interpolation as the input of wavelet packet decomposition. In order to preserve the characteristics of the regional point cloud data, the number of data that the selected rectangle contains should be as large as possible.

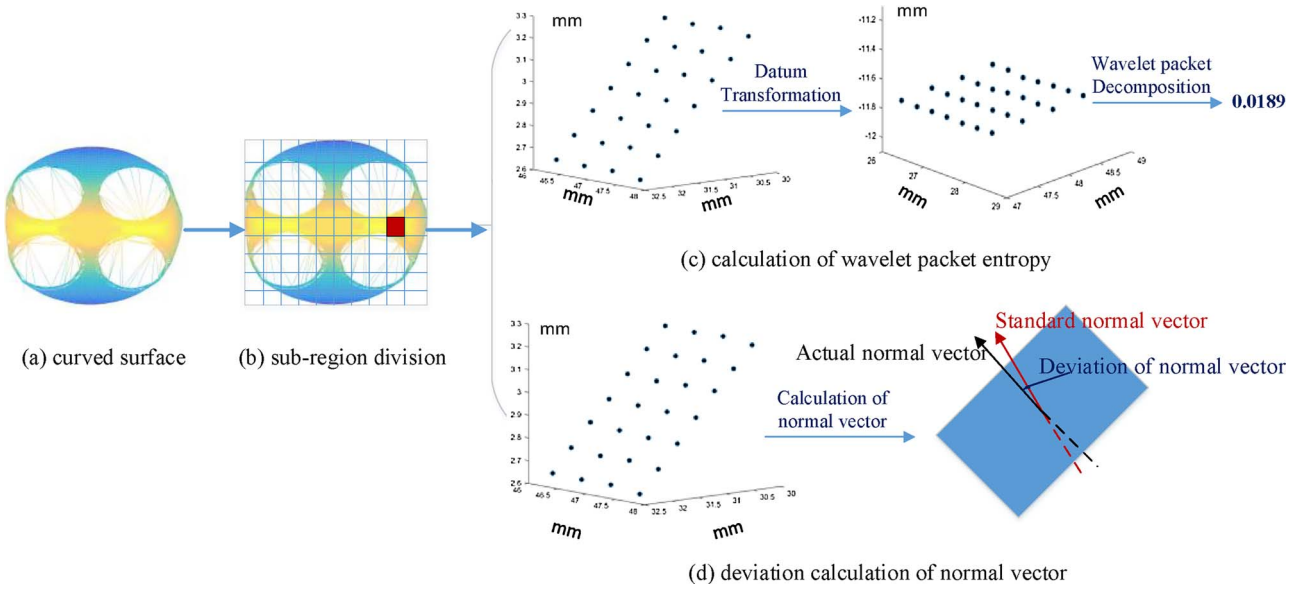

Fig. 10. Calculation of NDAP and PDD of a sub-region.

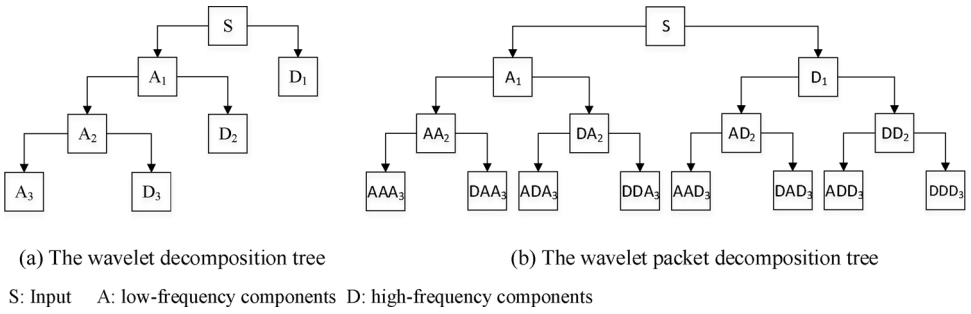

Fig. 11. The decomposition trees of wavelet and wavelet packet.

Step 2.1: Identify the largest rectangular region that contains valid data. It can be seen from Fig. 13 that there are points marked as NaN (null value), which should not be included in the input data. Remove the rows/columns that only contains mark of NaN. The unit of data in Fig. 13 is millimeter (mm).

Step 2.2: Count the number of non-null data of each row/column, and delete the row/column that contains the least number of non-null data of all rows and columns until the data contained in each row/column is non-null (shown in Fig. 14). The unit of data in Fig. 14 is mm. If the number of rows to be deleted is too large, the column that contains the least number of non-null data should be deleted.

Step 3: Wavelet packet decomposition. The wavelet packet decomposition is a multi-level division of the frequency band, which further decomposes the high frequency components. It can adaptively select the corresponding frequency band to match the signal spectrum according to the characteristics of the analyzed data, and improve the time-frequency resolution. In this study, 2-D Wavelet packet is used to decompose the divided sub-regions. A two-layer decomposition tree of 2-D wavelet packet is shown in Fig. 15. The decomposition relationship is expressed as $S_{0,0} = S_{2,0} + S_{2,1} + S_{2,2} + S_{2,3} + S_{2,4} + S_{2,5} + S_{2,6} + S_{2,7} + S_{2,8} + S_{2,9} + S_{2,10} + S_{2,11} + S_{2,12} + S_{2,13} + S_{2,14} + S_{2,15}$. The coefficient matrices of all nodes of the last layer are the output of wavelet packet decomposition.

Step 4: Calculation of wavelet packet entropy. The wavelet packet coefficient vector of the i^{th} scale is recorded as

$$\boldsymbol{S}_i = (S_{i,1}, S_{i,2}, ..., S_{i,j}) \tag{1}$$

where $S_{i,j}(j = 1,2,...,n)$ is the wavelet packet coefficient of the i^{th} scale. The coefficient vectors of all scales form a coefficient matrix $\{\boldsymbol{S}_i\}$, $i = 1,2, ...,m$, where m is the scale of wavelet packet

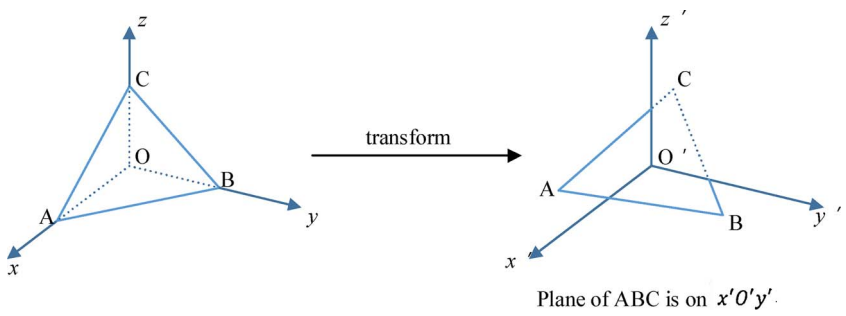

Fig. 12. Datum transformation of sub-region plane.

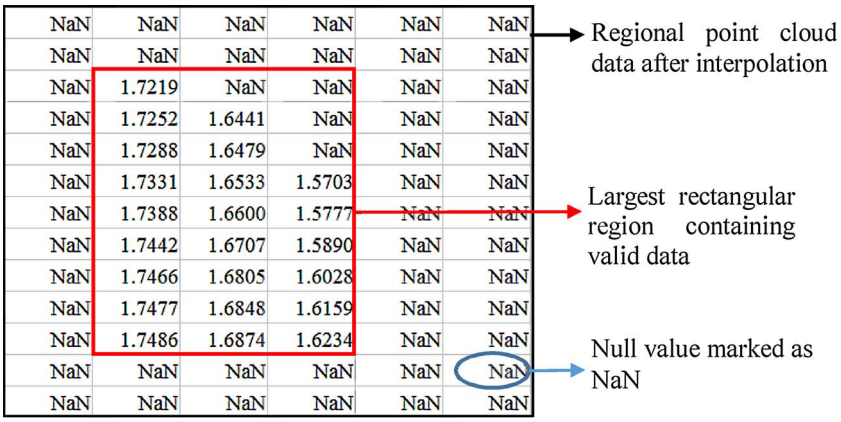

Fig. 13. Selection of largest rectangular region containing valid data.

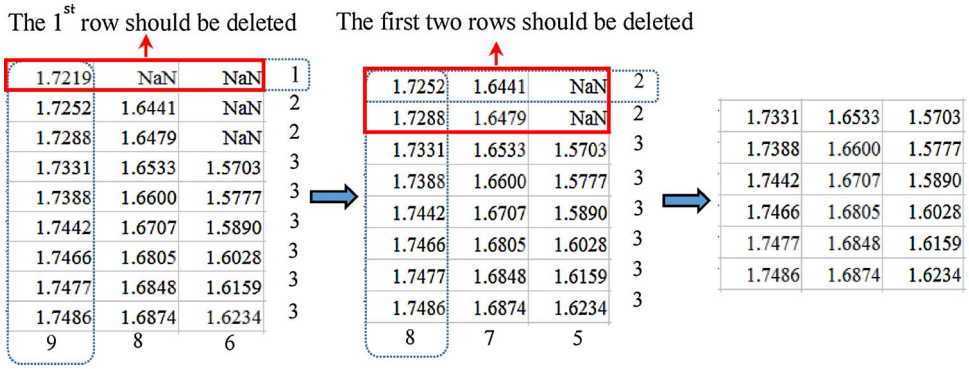

Fig. 14. Selection of rectangular region that only contains valid data.

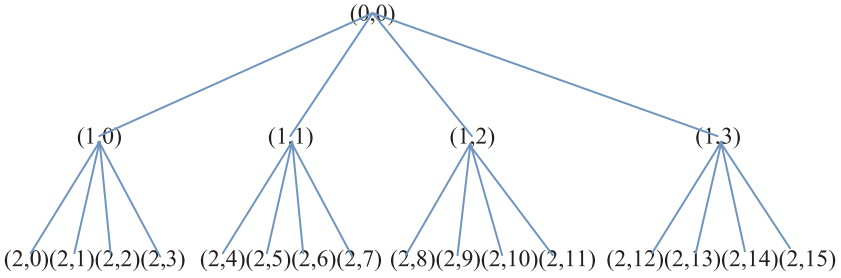

Fig. 15. A two-layer decomposition tree of 2-D Wavelet packet.

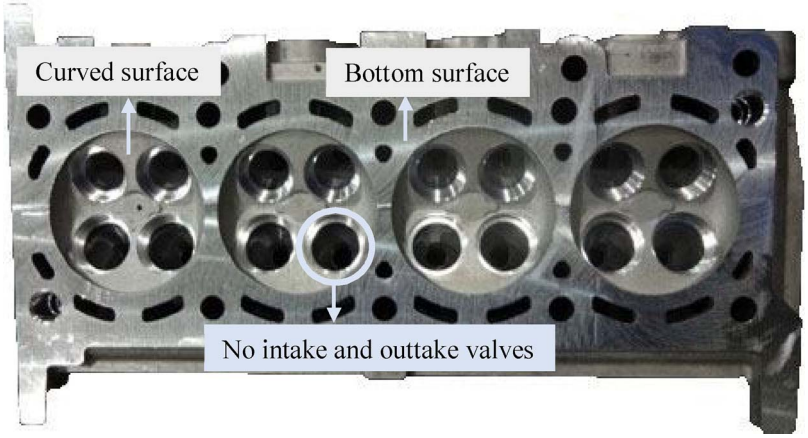

Fig. 16. Cylinder head of B12 engine with four combustion chambers.

(a) Measurement component (b) Industrial personal computer

Fig. 17. On-line measurement equipment based on HDM system.

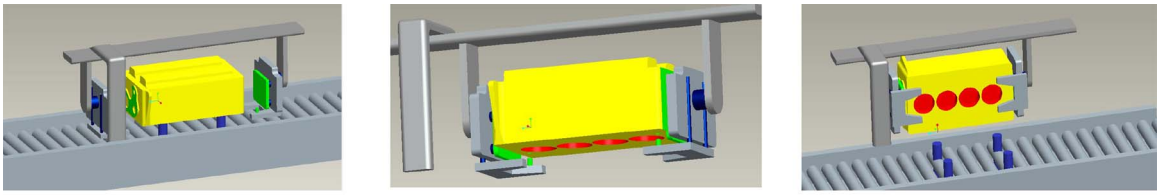

(a) Locate (b) Clamp (c) Flip over

Fig. 18. The measurement process.

decomposition. The norm vector of the wavelet packet coefficient matrix to measure the divided sub-region at each scale, that is, the energy of each scale is used to measure the proximity of the decomposed components of each scale. Normalize the energy vector E_i and analyze structure and complexity of the divided sub-region through distribution of the normalized energy vector. The energy of the i^{th}scale is defined as

$$E_i = S_i^2 = \sum_{j=1}^{n} |S_{i,j}|^2 \tag{2}$$

The distribution of energy vector is defined as the normalized energy at each scale

$$p_i = E_i/E \tag{3}$$

and the total energy is $E = \sum_{i=1}^{m} E_i$.

The entropy based on the energy distribution of each scale of the wavelet packet is called the wavelet packet entropy and its calculation is

$$WE = -\sum_{i=1}^{m} p_i \log_2(p_i) \tag{4}$$

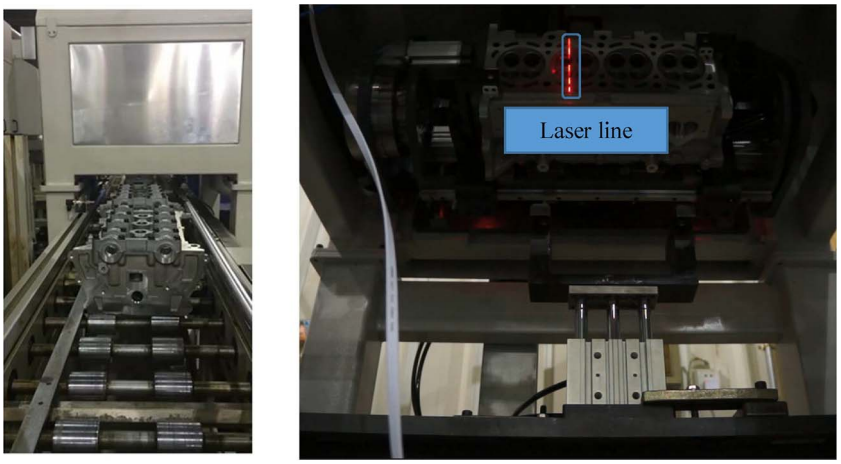

(a) On-line measurement (b) An example of measurement

Fig. 19. Actual operation of the on-line measurement equipment.

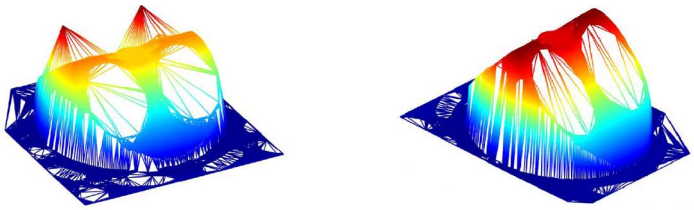

(a) Point cloud data before remove of outliers (b) Point cloud data after remove of outliers

Fig. 20. Point cloud data of a curved surface.

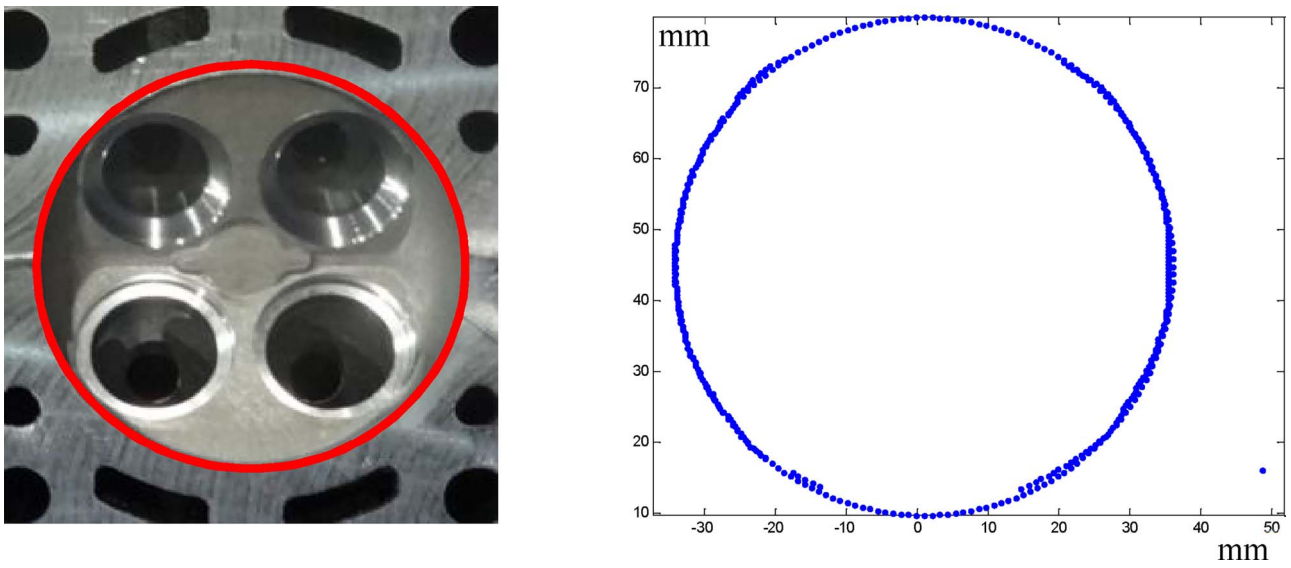

Fig. 21. Boundary of the curved surface.

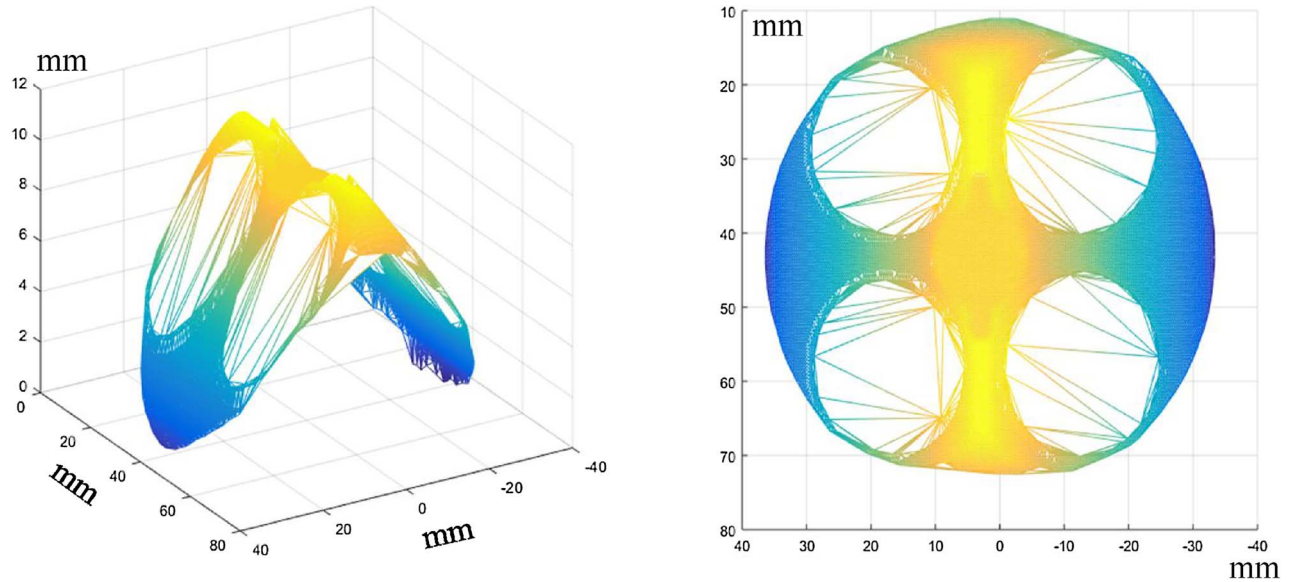

(a) Plot of the chamber point cloud data in 3-D coordinate system

(b) Plot of the chamber point cloud data in XY plane of 3-D coordinate system

Fig. 22. Point cloud data of the curved surface after boundary recognition.

2.3.2. Normal vector

The normal vector of each divided sub-region is regarded as the feature of the divided sub-regions. The plane parametric equation of $Ax + By + Cz + D = 0$ is calculated by fitting the divided regional point cloud data. Then the normal vector (A, B, C) of the divided sub-region is obtained and the steps are described as follows.

Step 1: Delete the points marked as [000] in each sub-region. Since the divided sub-regions conclude plane point cloud data, there may be

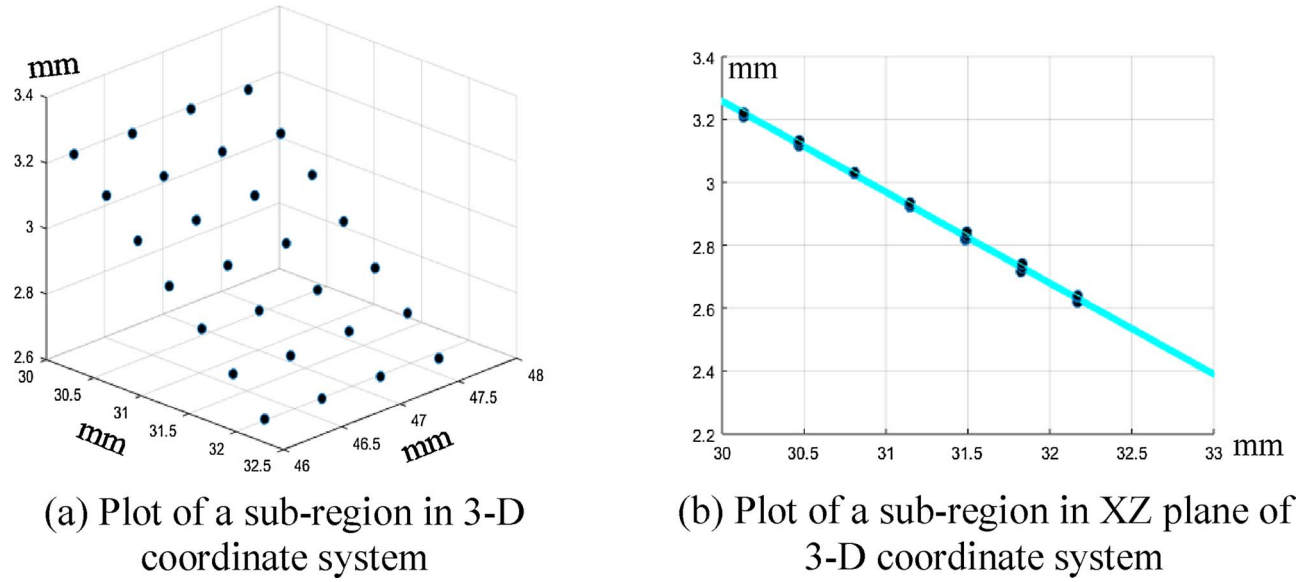

Fig. 23. Plot of points of a sub-region.

sub-regions that only contain [000] and these sub-regions should be marked with empty set instead of being deleted in order to ensure that the overall number of the divided sub-regions is not reduced.

Step 2: Count the number of remaining points in each sub-region. For the sub-region (effective sub-region) with the number of points larger than or equal to 3, the random sample consensus (RANSAC) algorithm [24,25] is used to fit the parametric equation of the effective sub-region and the normal vector is obtained.

2.4. Quality parameters calculation of curved surfaces

Before monitoring quality of the curved surface, the quality of the divided multiple sub-regions should be evaluated based on the wavelet packet entropies and normal vector errors. In order to calculate the wavelet packet entropy, the modulus point cloud data is needed. The modulus point cloud data is processed by boundary recognition, sub-region division and calculation of wavelet packet entropy. The wavelet packet entropies of the modulus point cloud data are regarded as the criteria to determine whether the corresponding sub-regions in the curved surface point cloud data is OOL. If the wavelet packet entropy of the curved surface point cloud data is larger than the wavelet packet entropy of the modulus point cloud data in the same sub-region, the sub-region of the curved surface is considered to be OOL. Similarly, the normal vector error is the angular deviation between the normal vector of the measured curved surface point cloud data and the normal vector of the modulus point cloud data in the same sub-region. If the angular deviation is larger than a threshold, the sub-region of the curved surface is considered to be OOL. The sub-region of the curved surface is determined to be OOL if either of wavelet packet entropy and the angular deviation of normal vector is OOL.

When OOL sub-regions of the curved surface are identified, the quality parameters that represent quality characteristics [15] of the curved surface are defined as: 1) the number of OOL sub-regions, 2) the number of OOL sub-regions of the largest cluster, 3) the number of clusters that contain OOL sub-regions more than a certain value. The last two quality parameters are calculated by a clustering algorithm [26] and the procedure of the clustering algorithm involves the following steps.

Step 1: Initialization and preprocessing. 1) Select the parameter t∈ (0,1) to determine the cutoff distance d_c. Usually, t ranges from 1% to 2%. 2) Calculate the distance ($dd_{i,j}$) between any two points, let $dd_{ji} = dd_{ij}$, $i < j$, $i, j \varepsilon I_S$. 3) Determine the cutoff distance d_c, which is used to determine the local density of each point in the data set. Sort the M_1 calculated distances in ascending order, and the order is expressed as$dd_1 \le dd_2 \le ... \le dd_{M_1}$. Here, $M_1 = \frac{1}{2}N_1(N_1 - 1)$, and N_1 is the number of all points. Let$d_c = dd_{f(M_1 t)}$, $f(M_1 t)$ represent an integer that is rounded to $M_1 t$. 4) Calculate the local density ($\{\rho_i\}_{i=1}^{N_1}$) of each point according to Eq. (1), and generate subscript sequencer ($\{q_i\}_{i=1}^{N_1}$) of the local densities in descending order.

$$\rho_i = \sum_{j \in I_S \setminus \{i\}} \chi(d_{ij} - d_c), \quad \chi(x) = \begin{cases} 1, & x < 0 \\ 0, & x \ge 0 \end{cases} \tag{5}$$

5) Calculate $\{\delta_i\}_{i=1}^{N_1}$and$\{n_i\}_{i=1}^{N_1}$. δ_i is the distance defined as

$$\delta_{q_i} = \begin{cases} \min\limits_{\substack{q_j \\ j<i}} \left\{ d_{q_i q_j} \right\} & i \ge 2 \\ \max\limits_{j \ge 2} \left\{ \delta_{q_j} \right\} & i = 1 \end{cases} \tag{6}$$

n_i is the serial number of points closest to x_i in the data points with local densities greater than x_i and is calculated by

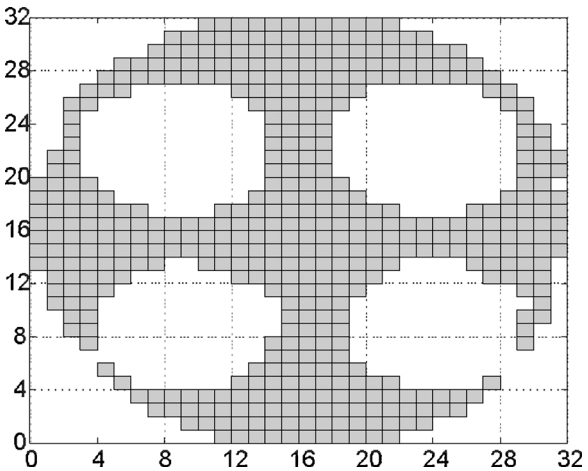

Fig. 24. Distribution of effective sub-regions.

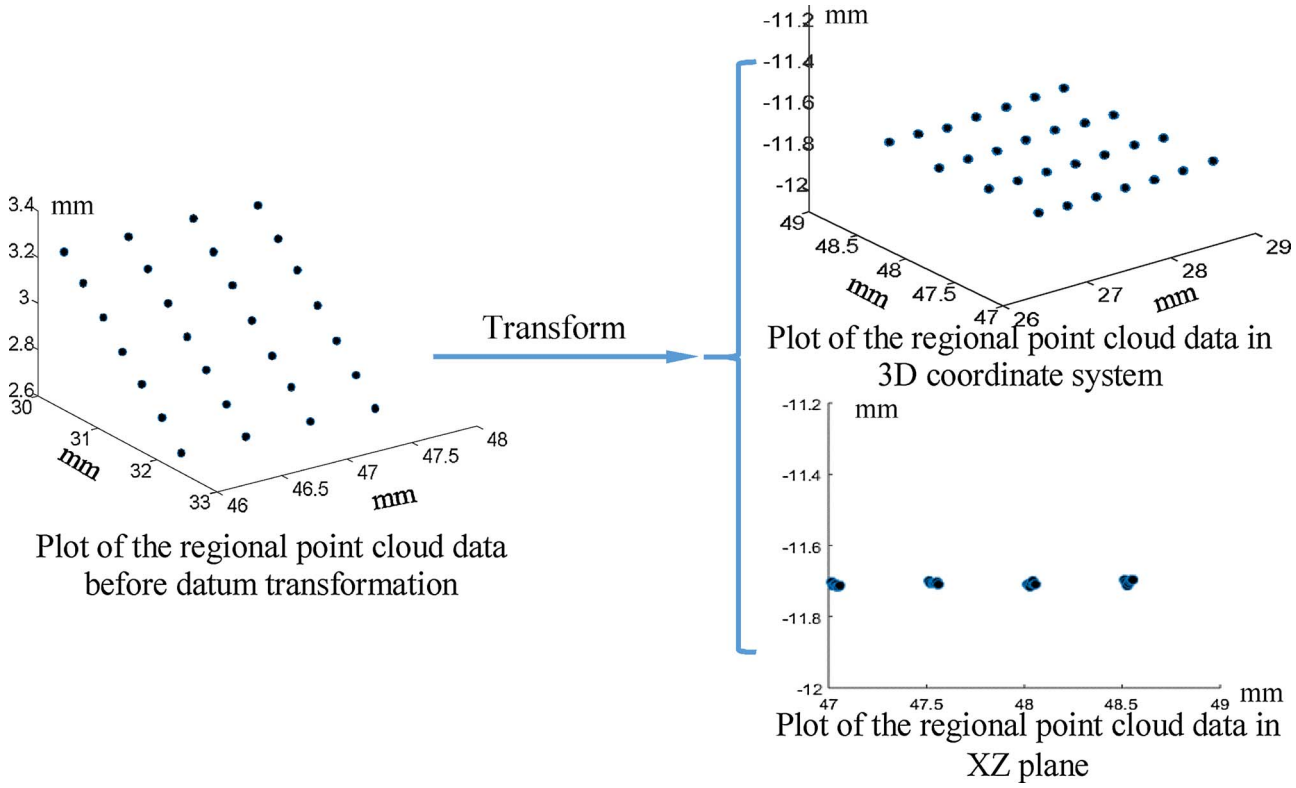

Fig. 25. Datum transformation of a sub-region.

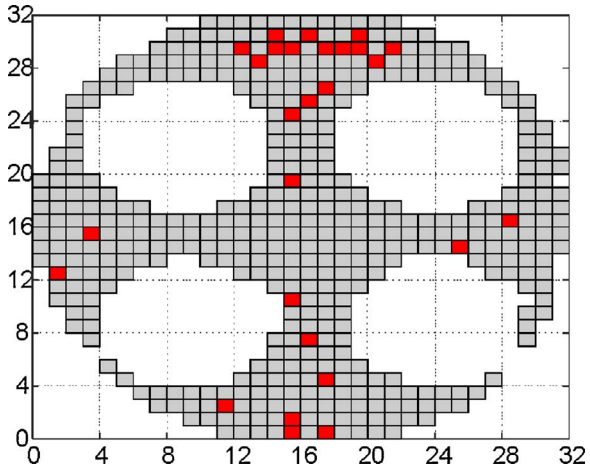

Fig. 26. OOL sub-regions in the curved surface.

$$n_{q_i} = \begin{cases} \arg\min\limits_{\substack{q_j \\ j<i}} \left\{ d_{q_i q_j} \right\} & i \geq 2 \\ 0 & i = 1 \end{cases} \tag{7}$$

Step 2: Determine the clustering center $\{m_j\}_{j=1}^{n_c}$ and initialize the category attribute tag ($\{c_i\}_{i=1}^{N}$) of the data point. c_i is determined by

$$c_i = \begin{cases} k, & x_i \text{is the cluster center and belongs to the } k^{th} \text{cluster} \\ -1, & \text{otherwise} \end{cases} \tag{8}$$

Step 3: Classify the non-clustering center points.

Step 4:If $n_c > 1$, further divide the data in each cluster into cluster core and cluster halo. 1) Initialize the tag $h_i = 0$, $i \in I_S$. 2) Generate an average local density upper bound $\{\rho_i^b\}_{i=1}^{n_c}$ for each cluster. 3) Identify cluster halo.

Step 5: The outputs are clusters and the corresponding clustering centers.

When the clusters of OOL sub-regions have been recognized, the quality parameters that represent quality characteristics of the curved surface are calculated by

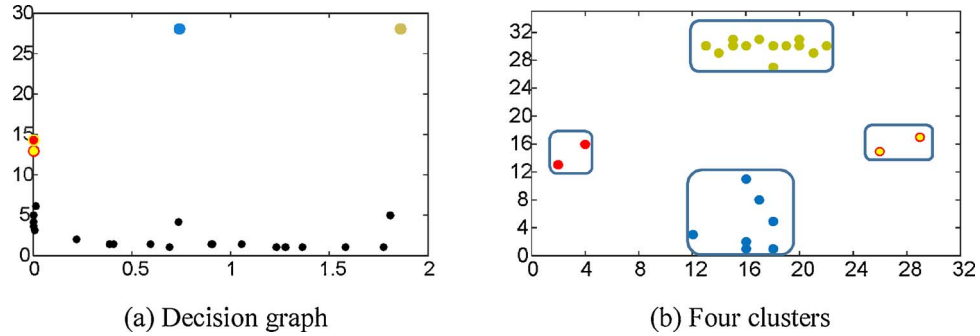

Fig. 27. The clustering result of an example of the curved surface.

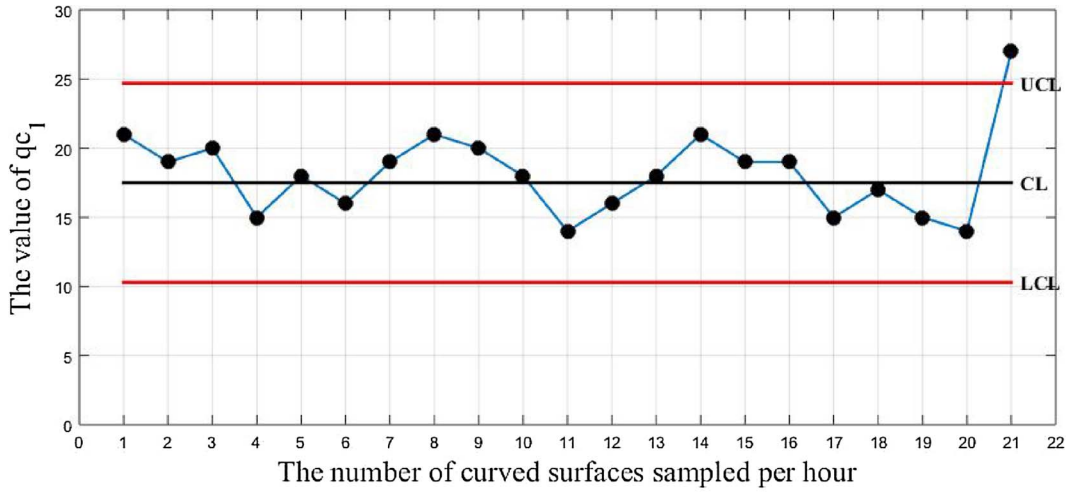

(a) monitoring of qc_1

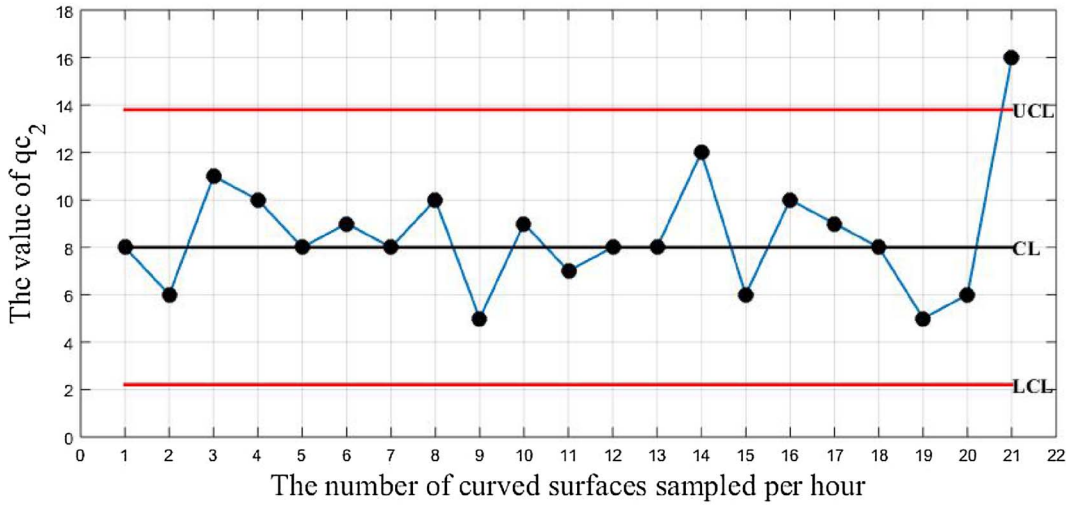

(b) monitoring of qc_2

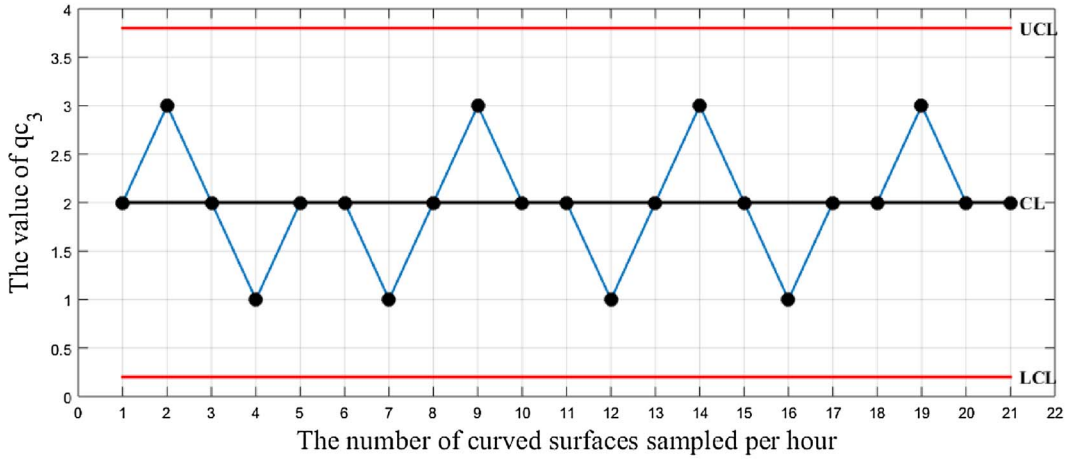

(c) monitoring of qc_3

Fig. 28. Curved surface defect monitoring.

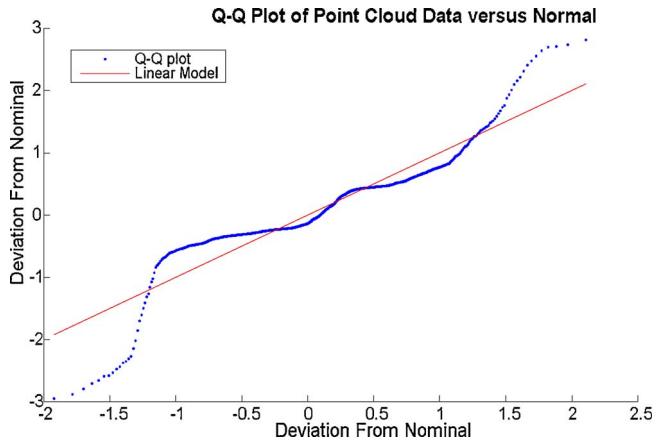

Fig. 29. Q–Q plot and fitted linear model for a curved surface in-control manufacturing process.

$$qc_1 = k_i \tag{9}$$

$$qc_2 = \max(N_{i,clust}) \tag{10}$$

$$qc_3 = \sum_{j=1}^{clust} S_j \tag{11}$$

where k_i is the number of OOL sub-regions of the i^{th} curved surface, *clust* is the number of clusters found on the curved surface, $N_{i,clust}$ is the size of the $clust^{th}$ cluster on the i^{th} surface, and S_j is a binary variable with a value of one when the j^{th} cluster has a size larger than s_c and zero otherwise.

2.5. Monitoring the quality parameters

The individual control chart is used in this monitoring phase. The centerline (CL), upper control limit (UCL) and lower control limit (LCL) of the individual control chart are determined by the following equation:

$$\begin{cases} CL = \mu \\ UCL = \mu + 3\sigma \\ LCL = \mu\text{-}3\sigma \end{cases} \tag{12}$$

where μ is mean and σ is standard deviation. μ and σ are estimated by

$$\mu = \frac{x_1 + x_2 + \ldots + x_n}{n} \tag{13}$$

$$\sigma = \sqrt{\frac{(x_1 - \mu)^2 + (x_2 - \mu)^2 + \ldots + (x_n - \mu)^2}{n}} \tag{14}$$

If an OOC condition is found, corrections (e.g. mold maintenance) should be conducted to ensure the quality of the consecutive curved surfaces. Otherwise, the manufacturing process of the curved surfaces should be kept.

3. Case study

In this case, the cylinder heads of B12 serial engines with four combustion chambers (see Fig. 16) are used to validate the performance of the proposed approach on detection and monitoring of defects on 3-D curved surface based on high-density point cloud data. Before the measurement, the intake and outtake valves are not put into the combustion chambers.

The point cloud data of combustion chambers of B12 engine cylinder heads is measured by an on-line HDM measurement machine using laser triangulation metrology [1]. Fig. 17 is the on-line measurement equipment. Fig. 18 exhibits the measurement process. Fig. 19 shows the actual operation of the on-line measurement equipment.

The field view of the HDM system is within 75 × 56 mm^2, and the depth of field view is 15 mm. Accuracy in X (translation direction) is ± 1 μm, accuracy in Y (direction of line laser) is ± 10 μm, and accuracy in Z is ± 20 μm. Resolution of the system is 0.02 mm^3. Repeatability is 0.02 ml. The HDM system is developed to measure the volumes of chambers. The outputs of the HDM system consist of the volume values and point clouds of the chamber. The design volume of the chambers is 24.4 ± 0.4ml, which indicates that the measurement error should be within 0.1 ml. Since the repeatability of the HDM system is 0.02 ml, the measurement error of the HDM system is allowable in the production process.

In this case, the moving speed of the guide rail is set at 10 mm/s, the acquisition frame rate of the 3-D measurement sensors is 110 f/s. The scan time of the cylinder head depends on the length of the cylinder head and speed of guide rail. The scan time of the cylinder head is 32s. Besides, the measurement time also includes time of grab (20 s), drop (15 s), and leave (10 s). Therefore, the total measurement time is 77 s, which is less than the cycle time 87.5 s of manufacturing a cylinder head, and the on-line measurement is easily implemented. The measurement time of the system is adjustable, and faster measurement can be achieved by increasing the speed of guide rail and acquisition speed of the system. 640 × 1280 is the number of points that are collected from a cylinder head by the HDM system. It includes the bottom surface and all chambers of a cylinder head. There are 640 points on a laser line and the total measurement contains 1280 laser lines. During the measurement, coordinates of the missing points are represented by specific coordinates and these specific coordinates are same. The points with same coordinate are regarded as missing points since coordinates of effective points are different.

3.1. Region division of curved surfaces

In this case, the curved surface of only a chamber is considered. In order to remove the outliers generated by ambient light interference, the maximum Z coordinate value is set as 11 cm (the maximum value is obtained by actual measurement). The threshold for removing outliers caused by the reflective properties of the curved surface of the workpiece is determined as 15 since a group of points less than 15 are considered to be isolated. The result of removing outliers is shown in Fig. 20. Boundary extraction of the curved surface is conducted and the result is shown in Fig. 21. The point cloud data of the curved surface (an inner surface of the chamber) is shown in Fig. 22. The of the In order to obtain as many small sub-regions as possible, the curved surface is divided into 32 × 32 sub-regions and a sub-region of them is shown in Fig. 23. It can be seen from Fig. 23(b) that the divided sub-region is similar to a plane. The unit of the axes in Fig. 21, Fig. 22 and Fig. 23 is mm.

3.2. Feature evaluation of each sub-region

After the region division of the curved surface, the effective sub-regions should be selected since there are sub-regions that are in the intake and outtake valve holes of the chamber inner surface. The sub-regions containing less than three points are marked as empty sub-regions and the distribution of the effective sub-regions is shown in Fig. 24. Before calculation of the wavelet packet entropies and normal vectors of the effective sub-regions, datum transformation of each sub-region is conducted and the result is shown in Fig. 25. The unit of the axes in Fig. 25 is mm.

The wavelet packet entropies and the normal vectors of the sub-regions of the modulus point cloud data are calculated as the criteria to evaluate whether sub-regions of the curved surface point cloud data are qualified. The wavelet packet entropies of some sub-regions are shown in Table 1 and the normal vector deviations of the same sub-regions are shown in Table 2.

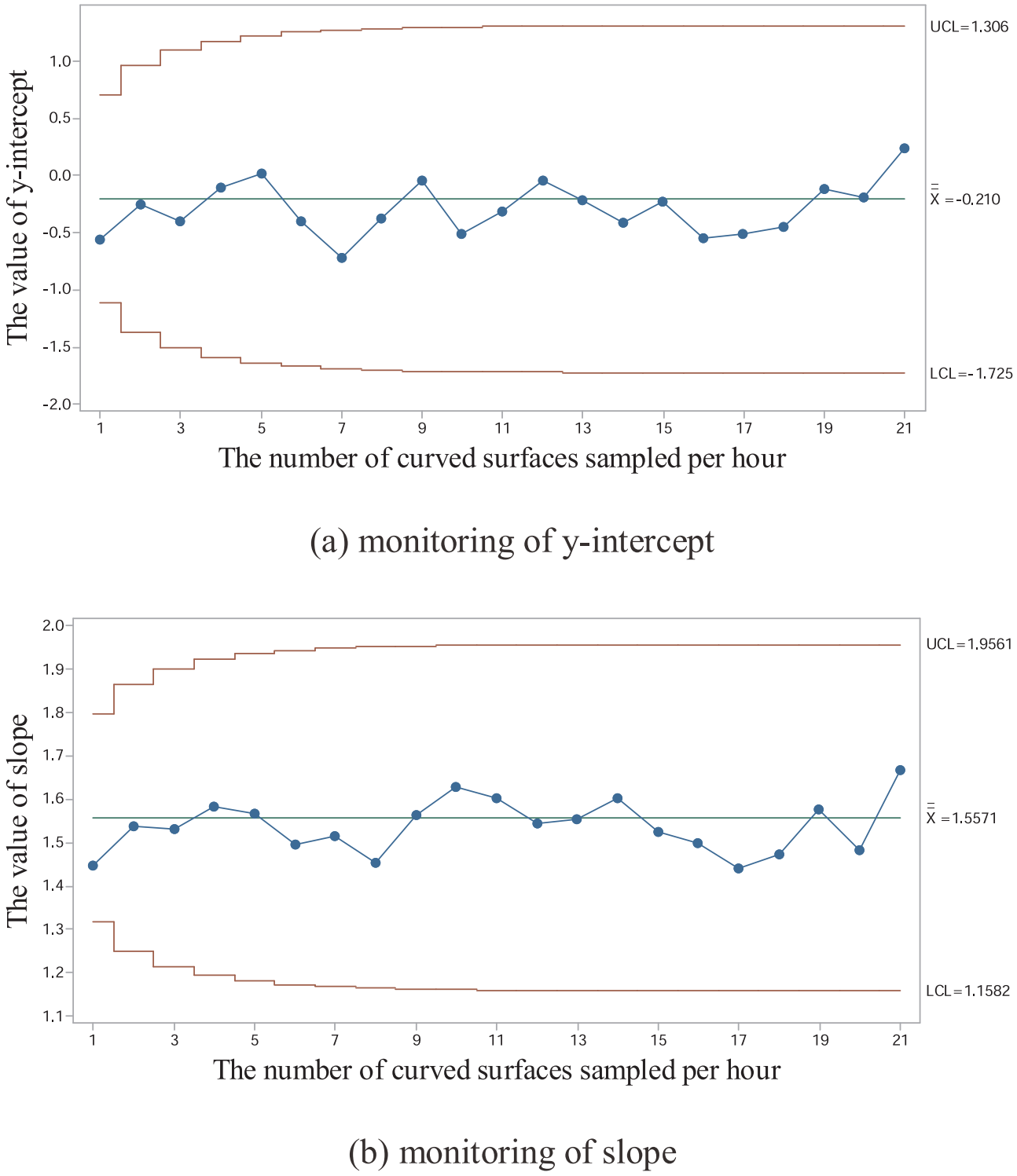

Fig. 30. Two EWMA control charts for monitoring y-intercept and slope.

In Table 1, the wavelet packet entropy of each measured sub-region is larger than the corresponding modulus sub-region. The reason is that the quality of the curved surface is inferior to quality of the designed modulus due to the errors in the manufacturing process. Therefore, it is not reasonable to use the wavelet packet entropies of the modulus sub-regions as the absolute limit to determine whether the sub-regions of the curved surface are OOL. A threshold value should be added to the limit of each sub-region. In this case, the threshold value is set as 0.5. That is, if the wavelet packet entropy difference of the curved surface sub-region and its corresponding modulus sub-region is larger than 0.5, the sub-region of the curved surface is considered to be OOL.

In Table 1, the 8th sub-region is an OOL sub-region. The limit of deviation degree is set as 0.5 based on engineering experience and there are two sub-regions (6th and 10th sub-region) are regarded as OOL in Table 2. Therefore, the 6th, 8th, and 10th sub-regions are OOL regions of the 14 sub-regions. An example of the curved surface that contains OOL sub-regions is shown in Fig. 26 and the OOL sub-regions are marked with red.

Table 1
Wavelet packet entropies of sub-regions of the curved surface and modulus.

Sub-region \index	1	2	3	4	5	6	7
Measured sub-region	0.0189	0.0169	0.0207	0.0272	0.0234	0.0226	0.0184
Modulus sub-region	0.0177	0.0155	0.0216	0.0240	0.0228	0.0145	0.0135
Sub-region \index	8	9	10	11	12	13	14
Measured sub-region	0.1085	0.0226	0.0292	0.0254	0.0220	0.0271	0.0229
Modulus sub-region	0.0243	0.0209	0.0256	0.0137	0.0172	0.0135	0.0139

3.3. Quality parameters calculation of curved surfaces

Once the OOL sub-regions in the curved surface are identified, three quality parameters that represent quality characteristics of the curved surface are quantified by numerical values. For the example shown in Fig. 26, the number of OOL sub-regions is 27. Since the values in Fig. 26 and Fig. 27 represent count values, there are no units for the axes in the two figures. Therefore, the first quality parameter is $qc_1 = 27$. The second quality parameter qc_2 is calculated by the clustering algorithm described in sub-section 2.4 and the clustering result is shown in Fig. 27. It can be seen from Fig. 27 (b) that the cluster marked with green contains the largest number (the number is 16) of bad sub-regions. Then the second quality parameter is $qc_2 = 16$. The numbers of OOL sub-regions in the four clusters are 16, 7, 2, and 2, respectively. For the curved surface of a chamber, the number of effective sub-regions is about 500 under the region division of 32 × 32. The threshold s_c is determined to be 3 based on engineering experience, which means that a cluster containing more than 3 OOL sub-regions is considered. In the example, there are 2 clusters containing more than 3 OOL sub-regions. Thus, the third quality parameter is $qc_3 = 2$.

3.4. Monitoring the quality parameters

In order to monitor the condition of the curved surface of chambers, three individual control charts are conducted to monitor the three quality parameters. In this case, 20 combustion chambers of qualified volumes are randomly sampled with time series and the point cloud data of the 20 curved surfaces are collected. The point cloud data is processed by procedures mentioned in Sub-section 2.2, 2.3 and 2.4. The values of three quality parameters of the 20 curved surfaces are shown in Table 3.

The CL, UCL, and LCL of three individual control charts are calculated according to Eqs. (15)–(17). Then the three individual control charts are conducted and shown in Fig. 28. There are no units for the y-axes in Fig. 28 since the three parameters are of no units.

$$\begin{cases} CL_{qc_1} = \mu_1 = \frac{\sum_{i=1}^{20}(qc_1)_i}{20} = 17.5 \\ UCL_{qc_1} = \mu_1 + 3\sigma_1 = \mu_1 + 3\sqrt{\frac{\sum_{i=1}^{20}((qc_1)_i - \mu_1)^2}{20}} = 17.5 + 3 \times 2.4 = 24.7 \\ LCL_{qc_1} = \mu_1 - 3\sigma_1 = \mu_1 - 3\sqrt{\frac{\sum_{i=1}^{20}((qc_1)_i - \mu_1)^2}{20}} = 17.5 - 3 \times 2.4 = 10.3 \end{cases} \tag{15}$$

$$\begin{cases} CL_{qc_2} = \mu_2 = \frac{\sum_{i=1}^{20}(qc_2)_i}{20} = 8 \\ UCL_{qc_2} = \mu_2 + 3\sigma_2 = \mu_2 + 3\sqrt{\frac{\sum_{i=1}^{20}((qc_2)_i - \mu_2)^2}{20}} = 8 + 3 \times 1.9 = 13.7 \\ LCL_{qc_2} = \mu_2 - 3\sigma_2 = \mu_2 - 3\sqrt{\frac{\sum_{i=1}^{20}((qc_2)_i - \mu_2)^2}{20}} = 8 - 3 \times 1.9 = 2.3 \end{cases} \tag{16}$$

$$\begin{cases} CL_{qc_3} = \mu_3 = \frac{\sum_{i=1}^{20}(qc_3)_i}{20} = 2 \\ UCL_{qc_3} = \mu_3 + 3\sigma_3 = \mu_3 + 3\sqrt{\frac{\sum_{i=1}^{20}((qc_3)_i - \mu_3)^2}{20}} = 2 + 3 \times 0.6 = 3.8 \\ LCL_{qc_3} = \mu_3 - 3\sigma_3 = \mu_3 - 3\sqrt{\frac{\sum_{i=1}^{20}((qc_3)_i - \mu_3)^2}{20}} = 2 - 3 \times 0.6 = 0.2 \end{cases} \tag{17}$$

In Fig. 28, parameters of the 21th curved surface are $qc_1 = 27$, $qc_2 = 16$, and $qc_3 = 2$. It can be seen that qc_1 and qc_2 are both out of the control range, and qc_3 is in the control range. Therefore, the manufacturing process of the curved surface is OOC. If there appears continuous OOC manufacturing process of curved surfaces, the correction should be conducted. For the bad sub-regions of curved surfaces of combustion chambers in this case, the main reason is that the mold of the chamber is worn and mold maintenance is needed.

In order to evaluate the detection accuracy of the proposed approach, 10 OOC conditions are recorded and the entire mold is inspected to find the bad sub-regions. Assume that the number of bad sub-regions of the mold is U_1, the number of the same bad regions of the mold and the curved surface is U_2. Then the detective accuracy is calculated by Eq. (18) and the detective accuracy of the proposed approach is shown in Table 4.

$$\text{Detceteveaccuracy} = \frac{U_1}{U_2} \times 100\% \tag{18}$$

According to Table 3, the average detective accuracy of the proposed approach is 83.95%. The detective accuracy and average detective accuracy can satisfy requirements of the mold maintenance. It is not necessary to inspect the entire mold since the defective sub-regions of the mold can be identified by the OOL sub-regions of the curved surfaces.

Table 2
Normal vector deviations of sub-regions of the curved surface.

Index\sub-region	Measured sub-region	Modulus sub-region	Deviation(degree)
1	(−0.398, −0.004, −1)	(−0.399, −0.003, −1)	0.073
2	(−0.288, −0.008, −1)	(−0.292, −0.011, −1)	0.268
3	(−0.289, −0.007, −1)	(−0.291, −0.007, −1)	0.106
4	(−0.305, −0.002, −1)	(−0.302, −0.003, −1)	0.167
5	(0.004, 0.002, −1)	(0.003, −0.002, −1)	0.237
6	(0.511, −0.021, −1)	(0.509, −0.011, −1)	0.518
7	(0.261, 0.011, −1)	(0.258, 0.009, −1)	0.195
8	(0.341, −0.0003, −1)	(0.342, 0.0007, −1)	0.075
9	(0.272, −0.001, −1)	(0.268, 0.003, −1)	0.308
10	(0.398, −0.014, −1)	(0.369, −0.009, −1)	1.472
11	(−0.280, −0.002, −1)	(−0.283, −0.003, −1)	0.169
12	(−0.302, −0.004, −1)	(−0.298, 0.001, −1)	0.346
13	(−0.013, −0.016, −1)	(−0.010, −0.014, −1)	0.207
14	(0.380, 0.003, −1)	(0.383, 0.005, −1)	0.184

Table 3
The values of three quality parameters of the 20 curved surfaces.

index	1	2	3	4	5	6	7	8	9	10
qc_1	21	19	20	15	18	16	19	21	20	18
qc_2	8	6	11	10	8	9	8	10	5	9
qc_3	2	3	2	1	2	2	1	2	3	2
index	11	12	13	14	15	16	17	18	19	20
qc_1	14	16	18	21	19	19	15	17	15	14
qc_2	7	8	8	12	6	10	9	8	5	6
qc_3	2	1	2	3	2	1	2	2	3	2

Table 4
The detective accuracy of the proposed approach.

Item \index	1	2	3	4	5	6	7	8	9	10
U_1	27	30	28	32	30	35	30	31	25	36
U_2	24	25	22	25	24	30	25	28	22	30
Detective accuracy (%)	88.9	83.3	78.6	78.1	80.0	85.7	83.3	90.3	88.0	83.3

The locations of OOL sub-regions on the curved surface corresponds to the locations of the mold to be inspected. Therefore, the mold maintenance only needs focus on checking the OOL sub-regions with fixed locations.

3.5. Comparison of the profile monitoring method based on Q–Q plot

In order to validate the performance of the proposed approach, the profile monitoring technique based on Q–Q plot [27,28] is used for comparison. For a process where a measured point cloud data is collected as a distribution of points, in-control point cloud data will produce highly linear Q–Q plot while out-of-control point clouds will result in a Q–Q plot deviating from linearity. Wang et al. [29] pointed out that this relationship could be monitored as a linear profile characterized by its y-intercept and slope, which can be monitored by two EWMA control charts. In this case, the data for Q–Q plot is the deviation of Z coordinate values of corresponding points (values of coordinate (x, y) should be the same) between the measured point cloud data and the modulus point cloud data. An example of Q–Q plot for a curved surface in-control manufacturing process is shown in Fig. 29. The monitoring of defects on three-dimensional curved surfaces is transforming into monitoring parameters (y-intercept and slope) of the fitted linear model. Two EWMA control charts for monitoring intercept and slope are shown in Fig. 30. There are no units for y-axes in Fig. 30 since the slope and y-intercept are represented by values without units.

It can be seen from Fig. 30 that the two parameters are within the control limits for the point cloud data of the 21 sampled curved surfaces, which indicates that the manufacturing process of the chambers is in control. However, the manufacturing process of the chambers is out of control from the 21th curved surface according to the result of the proposed method. It means that the monitoring method based on Q–Q plot are not able to identify OOC process in time when compared to the proposed method. The reason is that the positions of the measured points (represented by coordinate (x, y)) for different chambers may not be same due to the positioning error in measurement, and the number of the modulus point cloud data is equal to the number of the measured point cloud data. The corresponding points between the measured point cloud data and the modulus point cloud data are not in the same position (values of coordinate (x, y) are different), which results in inaccurate monitoring results. However, the curved areas of the modulus point cloud data and measured point cloud data are the same for sub-region division of the proposed method, and the divided sub-regions of the modulus point cloud data and measured point cloud data are one-to-one correspondence. Thus, the positions of the measured points have no effect on the monitoring result of the proposed method. Besides, there is no appropriate method to detect the location of the defects on the curved surface, since the spatial aspect of the data is lost when transforming the point cloud data into Q–Q plot. Therefore, the monitoring and detecting performance of the proposed method is superior to the profile monitoring method based on Q–Q plot.

4. Conclusions

This paper has developed a systematic approach for detection and monitoring of defects on 3-D curved surfaces based on high-density point cloud data, which consists of region division of curved surfaces, feature evaluation of each sub-region, quality parameters calculation of curved surfaces, and monitoring the quality parameters. The region division of curved surfaces is conducted to divide the curved surface into multiple sub-regions (each sub-region is similar to a plane) that are decomposed by wavelet packet. Wavelet packet entropy and normal vector are calculated to represent the NDAP and PDD features of the multiple sub-regions. Wavelet packet entropy and normal vector of the modulus point cloud data also need to be calculated as the criteria to determine whether sub-regions of the curved surface are OOL. When the OOL sub-regions are identified, three quality parameters that represent quality characteristics of the curved surface are calculated based on the clusters of the OOL sub-regions. Then, three individual control charts are proposed to monitor the three quality parameters. As long as any quality parameter is out of the control range, the manufacturing process of the curved surface is determined to be OOC. A case study of curved surfaces of cylinder head combustion chambers sampled in time series is conducted to validate performance of monitoring and detection of defects on curved surfaces. The results demonstrate that the proposed approach can identify the OOC manufacturing process of 3-D curved surfaces and accurately detect the locations of the OOL sub-regions from the curved surfaces in OOC manufacturing process. The comparison with other monitoring methods (for example, profile monitoring based on Q–Q plot) for high-density point cloud data of 3-D curved surfaces shows that the proposed method is more reliable when there exists positioning error in measurement, and shows good performance of identifying locations of defects.

Acknowledgments

The authors greatly acknowledge the editor and the reviewers for their valuable comments and suggestions that have led to a substantial improvement of the paper. This work was supported by the Major Program of the National Natural Science Foundation of China (Grant No. 51535007) and the National Natural Science Foundation of China (Grant No. 51775343).

References

[1] Huang D, Du S, Li G, Wu Z. A systematic approach for on-line minimizing volume difference of multiple chambers in machining processes based on high definition metrology. J Manuf Sci Eng 2017;139(8):081003.
[2] Wang K, Jiang W, Li B. A spatial variable selection method for monitoring product surface. Int J Prod Res 2016;54(14):4161–81.
[3] He Z, Zuo L, Zhang M, Megahed F. An image-based multivariate generalized likelihood ratio control chart for detecting and diagnosing multiple faults in manufactured products. Int J Prod Res 2016;54(6):1771–84.
[4] Sullivan J. Detection of multiple change points from clustering individual observations. J Qual Technol 2002;34(4):371–83.
[5] Woodall W, Spitzner D, Montgomery D, Gupta S. Using control charts to monitor process and product quality profiles. J Qual Technol 2004;36(3):309–20.
[6] Du S, Liu C, Huang D. A shearlet-based separation method of 3D engineering surface using high definition metrology. Precis Eng 2015;40:55–73.
[7] Du S, Liu C, Xi L. A selective multiclass support vector machine ensemble classifier for engineering surface classification using high definition metrology. J Manuf Sci Eng 2015;137(1):011003.
[8] Du S, Huang D, Wang H. An adaptive support vector machine-based workpiece surface classification system using high-definition metrology. IEEE Trans Instrum

Meas 2015;64(10):2590–604.
[9] Du S, Fei L. Co-kriging method for form error estimation incorporating condition variable measurements. J Manuf Sci Eng 2016;138(4):041003.
[10] Du S, Liu T, Huang D, Li G. A fast and adaptive bi-dimensional empirical mode decomposition approach for filtering of workpiece surfaces using high definition metrology. J Manuf Syst 2018;46:247–63.
[11] Wang M, Ken T, Du S, Xi L. Tool wear monitoring of wiper inserts in multi-insert face milling using three-dimensional surface form indicators. J Manuf Sci Eng 2015;137(3):031006.
[12] Wang M, Shao Y, Du S, Xi L. A diffusion filter for discontinuous surface measured by high definition metrology. Int J Precis Eng Manuf 2015;16(10):2057–62.
[13] Wang M, Xi L, Du S. 3D surface form error evaluation using high definition metrology. Precis Eng 2014;38(1):230–6.
[14] Suriano S, Wang H, Shao C, Hu S, Sekhar P. Progressive measurement and monitoring for multi-resolution data in surface manufacturing considering spatial and cross correlations. IIE Trans 2015;47(10):1033–52.
[15] Nguyen H, Wang H, Tai, Ren J, Hu S, Shih A. High-definition metrology enabled surface variation control by cutting load balancing. J Manuf Sci Eng 2016;138(2):021010.
[16] Wells L, Shafae M, Camelio J. Automated surface defect detection using high-density data. J Manuf Sci Eng 2016;138(7):071001.
[17] Wang K, Tsung F. Using profile monitoring techniques for a data-rich environment with huge sample size. Qual Reliab Eng Int 2005;21(7):677–88.
[18] Wells L, Megahed F, Niziolek C, Camelio J, Woodall W. Statistical process monitoring approach for high-density point clouds. J Intell Manuf 2013;24(6):1267–79.
[19] Colosimo B, Cicorella P, Pacella M, Blaco M. From profile to surface monitoring: SPC for cylindrical surfaces via Gaussian Processes. J Qual Technol 2014;46(2):95–113.
[20] Chen Q, Yang S, Li Z. Surface roughness evaluation by using wavelets analysis. Precis Eng 1999;23(3):209–12.
[21] Lu C, Troutman JR, Schmitz TL, Ellis J, Tarbutton J. Application of the continuous wavelet transform in periodic error compensation. Precis Eng 2016;44:245–51.
[22] Xu J, Yamada K, Seikiya K, Tanaka R, Yamane Y. Effect of different features to drill-wear prediction with back propagation neural network. Precis Eng 2014;38(4):791–8.
[23] Barnhill R, Opitz K, Pottmann H. Fat surfaces: a trivariate approach to triangle-based interpolation on surfaces. Comput Aided Geom Des 1992;9(5):365–78.
[24] Fischler M, Bolles R. Random sample consensus: a paradigm for model fitting with applications to image analysis and automated cartography. Commun ACM 1981;24(6):381–95.
[25] Raguram R, Chum O, Pollefeys M, USAC. A universal framework for random sample consensus. IEEE Trans Pattern Anal Mach Intell 2013;35(8):2022–38.
[26] Rodriguez A, Laio A. Clustering by fast search and find of density peaks. Science 2014;344(6191):1492–6.
[27] Du S, Lv J, Xi L. On-line classifying process mean shifts in multivariate control charts based on multiclass support vector machines. Int J Prod Res 2012;50:6288–310.
[28] Du S, Lv J. Minimal Euclidean distance chart based on support vector regression for monitoring mean shifts of auto-correlated processes. Int J Prod Econ 2013;141:377–87.
[29] Wang K, Tsung F. Using profile monitoring techniques for a data-rich environment with huge sample size. Qual Reliab Eng Int 2005;21(7):677–88.